The changeable power-law singularity and its application to prediction of catastrophic rupture in uniaxial compressive tests of geo-media

Jian Xue[1,2], Shengwang Hao[3,1], Jun Wang[1], Fujiu Ke[4], Chunsheng Lu[5], and Yilong Bai[1,2]

[1]State Key Laboratory of Nonlinear Mechanics (LNM), Institute of Mechanics, Chinese Academy of Sciences, Beijing, China. [2]School of Engineering Science, University of Chinese Academy of Sciences, Beijing, China. [3]School of Civil Engineering and Mechanics, Yanshan University, Qinhuangdao, China. [4]School of Physics and Nuclear Energy Engineering, Beihang University, Beijing, China. [5]School of Civil and Mechanical Engineering, Curtin University, Perth, Australia.

Corresponding author: Shengwang Hao (hsw@ysu.edu.cn)

Key Points:

- The exponent of power-law singularities ranges from −1/2 to −1.
- A reduced power-law exponent monotonically decreases to its lower limit.
- Catastrophic rupture can be predicted with the changeable power-law exponent.

This article has been accepted for publication and undergone full peer review but has not been through the copyediting, typesetting, pagination and proofreading process which may lead to differences between this version and the Version of Record. Please cite this article as doi: 10.1002/2018JB015591

Abstract

The acceleration precursor of catastrophic rupture in rock-like materials is usually characterized by a power-law relationship, but the exponent exhibits a considerable scatter in practice. In this paper, based on experiments of granites and marbles under quasi-static uniaxial and unconfined compression, it is shown that the power-law exponent varies between −1 and −1/2. Such a changeable power-law singularity can be justified by the energy criterion and a power function approximation. As the power-law exponent is close to the lowest value of −1, rocks are prone to a perfect catastrophic rupture. Furthermore, it is found that the fitted reduced power-law exponent decreases monotonically in the vicinity of a rupture point and converges to its lower limit. Therefore, the upper bound of catastrophic rupture time is constrained by the lowest value of the exponents and can be estimated in real-time. This implies that, with the increase of real-time sampling data, the predicted upper bound of catastrophic rupture time can be unceasingly improved.

1. Introduction

The accelerating behavior of some response quantities (e.g., deformation and seismic events) is widely observed before natural disasters such as volcanic eruptions [*Voight*, 1988; *Kilburn and Voight*, 1998; *Kilburn*, 2003; *Bell et al.*, 2011; *Bell et al.*, 2013; *Boué et al.*, 2015; *Hao et al.*, 2016], landslides [*Helmstetter et al.*, 2004], and earthquakes, as well as in rupture experiments [*Nechad et al.*, 2005a; *Heap et al.*, 2009; *Hao et al.*, 2013; *Hao et al.*, 2014]. This has been analyzed as a critical phenomenon [*Bak and Tang*, 1989; *Toussaint and Pride*, 2002a, 2002b, 2002c; *Rundle et al.*, 2003; *Toussaint and Pride*, 2005; *Girard et al.*, 2010; *Abaimov and Cusumano*, 2014] with a power-law divergence of macroscopically observable quantities [*Guarino et al.*, 1998; *Rundle et al.*, 2000; *Guarino et al.*, 2002; *Weiss et al.*, 2014] at failure. Such an accelerating behavior is usually accepted as a precursor for prediction of time-to-failure [*Voight*, 1988; 1989; *Kilburn and Voight*, 1998; *Main*, 1999; *Kilburn*, 2003; 2012; *Hao et al.*, 2016]. For example, to quantitatively describe an acceleration process during the evolution to failure, *Voight* [1988; 1989] suggested an empirical relationship, that is

$$\ddot{\Omega}\dot{\Omega}^{-\alpha} = A, \tag{1}$$

where Ω is a response quantity (e.g., deformation, cumulative energy release, acoustic emission etc.), α is an exponent measuring the degree of non-linearity [*Main*, 1999], and A is a constant. The dot represents the first and second derivatives of the response with respect to time. Quantities that might be represented by Ω include deformation or strain of rocks,

conventional geodetic observations (e.g., fault slip, strain, length or angular change), seismic quantities such as Benioff strain, which is defined as the square root of cumulative energy release [*Voight*, 1988].

Voight's relation (equation (1)) has been justified by comparison with equations for quasi-static, subcritical crack growth [*Kilburn and Voight*, 1998]. Voight's relation in predicting failure time is known as the failure forecast method [*Kilburn and Voight*, 1998; *Kilburn*, 2003; *Bell et al.*, 2011; *Bell et al.*, 2013], which has been widely validated by the retrospective prediction of volcanic eruptions [*Voight*, 1988; *Kilburn and Voight*, 1998; *Kilburn*, 2003], earthquake [*Bufe and Varnes*, 1993; *Bowman et al.*, 1998; *Main*, 1999], and laboratory data [*Lavallée et al.*, 2008; *Smith et al.*, 2009]. In these applications, a power-law relationship of the response rate can be derived as

$$\dot{\Omega} = K\left(t_f - t\right)^r , \qquad (2)$$

where t_f is the failure time, $K = [A(\alpha - 1)]^{1/(1-\alpha)}$, and $r = -1/(\alpha - 1)$ [*Voight*, 1988], which was verified in creep [*Nechad et al.*, 2005b; *Heap et al.*, 2009] and creep-relaxation experiments of rocks [*Hao et al.*, 2014]. To extend these analyses to deformation under increasing stress, *Kilburn* [2012] suggested an alternative expression of Voight's relationship to describe precursory time series. Then, based on uniaxial compressive experiments of granites and marbles as illustrated in Figure 1, *Hao et al.* [2013] introduced a response function $R = du/dU$, defined as the change of sample's deformation u with respect to the crosshead displacement U of a testing machine. Their experimental results showed that, approaching to catastrophic

rupture, the response function increases as a power-law function

$$R = B_{\mathrm{F}}\left(1 - U/U_{\mathrm{F}}\right)^{\beta_{\mathrm{F}}}, \tag{3}$$

where B_{F} is a constant, β_{F} is an exponent, subscript F represents the value at a failure point, and U is a displacement combination of the sample and load apparatus (Figure 1).

When the exponent r (or β_{F}) is equal to −1 (i.e., $\alpha = 2$ in Voight's relation), the reciprocal of R has a linear relationship with the controlling displacement U. Then, as illustrated in Figure 2, by linearly extrapolating the inverse rate to zero [*Kilburn and Voight*, 1998; *Kilburn*, 2003; *Lavallée et al.*, 2008; *Smith et al.*, 2009], failure time can be determined as the intersection point with the abscissa axis [*Voight*, 1988; 1989; *Voight and Cornelius*, 1991; *Cornelius and Scott*, 1993; *Cornelius and Voight*, 1994; *Sornette and Sammis*, 1995; *Kilburn and Voight*, 1998; *Kilburn*, 2003; *Helmstetter et al.*, 2004; *Smith and Kilburn*, 2010; *Bell et al.*, 2013; *Hao et al.*, 2016]. This method works well in retrospective analysis of landslides and volcanic eruptions [*Voight*, 1988; *Cornelius and Voight*, 1994; *Kilburn and Voight*, 1998].

It is worth noting that, however, the power-law exponent r (or β_{F}) is not always equal to −1, and according to a number of experiments, there is a large dispersion in its value [*Voight and Cornelius*, 1991; *Kilburn*, 2003; 2012; *Boué et al.*, 2015]. In the case of creep damage, *Cornelius and Scott* [1993] reported that the exponent α in Voight's relation is between 1.47 and 2.12. *Voight* [1989] found out that $1.74 < \alpha < 2.01$ for metals and $1.9 < \alpha < 2.1$ for soil. *Rundle et al.* [2000] derived an exponent of 1/4 based on the first-order phase transition. In addition, observations indicate that the exponent is about 0.3 for large earthquakes [*Bufe et al.*,

1994; *Main*, 1999; *Ben-Zion and Lyakhovsky*, 2002]. *Hao et al.* [2013] showed that the average value of power exponents is −0.51. Thus, it is pivotal to have a better understanding on the variation of power-law exponents.

A system consisting of the load apparatus (represented by a linear spring in Figure 1) and a slipper or damageable sample in series [*Brace and Byerlee*, 1966; *Salamon*, 1970; *Hudson et al.*, 1972; *Jaeger and Cook*, 1979; *Li and Rice*, 1983; *Hao et al.*, 2012] is usually used to simulate the process of elastic energy release inducing catastrophic rupture in rocks. Similar models [*Lyakhovsky et al.*, 2011; *Lyakhovsky and Ben-Zion*, 2014] have been developed to describe the transition from the quasi-static evolution to dynamic slip events. Energy release from surroundings driving catastrophic rupture of a damage zone is a significant mechanism of natural disasters such as earthquakes [*Brace and Byerlee*, 1966; *Li and Rice*, 1983; *Scholz*, 1998, *Carpenter et al.*, 2011], pillar failure [*Salamon*, 1970], and displacement in underground structures.

In this paper, quasi-static uniaxial and unconfined compression experiments are carried out to simulate the energy release inducing catastrophic rupture and investigate the power-law acceleration of the response function R (equation (3)) in the vicinity of catastrophic rupture. Rock samples are tested by monotonically and quasi-statically moving the crosshead of a testing machine. Then, power-law exponents are determined by experimental results and an analytic reasoning with a power function approximation. In particular, the variation of β_{F} is discussed in terms of an energy criterion. Finally, the real-time evolution of a reduced

power-law exponent approaching to β_F is adopted to develop a method to estimate the constraint on warning of catastrophic rupture.

2. Samples and experimental method

Two kinds of granites and marbles were cut into prismatic blocks with 40 mm in height (see Table 1 for their sizes in cross-section). The aspect ratio of a sample was not less than 2. The same kind of rock samples was taken from a complete, generally uniform rock with the same sampling direction. All the samples were intact (see Figure S1 in Supporting Information), but with inevitable and randomly distributed micro-defects. Then, the surface of each sample was polished and smoothed to ensure that the end face of a sample was flat and perpendicular to its height axis with the verticality of < 0.001 rad. To avoid the influence of moisture content of a sample on its uniaxial compressive strength and catastrophic rupture, all the cleaned samples were placed in an electric oven and dried at 105 ± 3 °C for 24 hours. After rock samples were cooled, they were quickly transferred to a dryer for storage, ensuring that all samples were in an almost absolute dry initial state prior to experiments. These samples were tested at temperatures ranging from 10 to 30 °C. The average relative room humidity was ~62%. The total number, size, initial stiffness and density of each kind of samples are listed in Table 1, and Figure 3 shows their optical microscope images and corresponding internal micro-structures.

In experiments, unconfined rock samples were uniaxially compressed along the height axis by using an MTS 810 material testing system (Figures 4a and 4b) with a stiffness of 210 kN/mm. The experimental procedure is illustrated in Figure 4c. It is seen that the controlling displacement on the crosshead, *U*, was input into the testing system by a computer and was successively calibrated by a servo controller according to feedback signals during loading (see Figure 4c). The displacement *U* was applied upward monotonically at a speed less than 1 mm/min (see Figures 4b and 4c), which was continuously measured by a linear variable differential transformer (LVDT) with a resolution of 1 μm, and the beam of the testing machine was fixed (see Figures 4a and 4c). The deformation *u* of a sample was tested by using a 1 μm resolution extensometer located on its side (see Figures 4b and 4c). The load was monitored by a force sensor with an offset load of 1 kN. Figure 4d shows the input signal *U* and the output curves. Here, it is worth noting that the deformation, *u*, of a sample increases rapidly in the vicinity of catastrophic rupture, which is associated with a jump of stress.

In the present tests, we take advantage of the plane surface of prismatic samples to monitor the evolution of a strain field. In order to reduce the stress concentration that may occur at the corners of a rock sample, the interface between the sample and the steel platen of the MTS testing machine was carefully treated to ensure uniaxial loading. It is shown that rupture modes are usually shearing under compression (see Figure 5).

In laboratory tests, the loading system consists of a load apparatus and a deformed sample. The displacement U of the crosshead of the testing machine includes the deformation of both load apparatus and rock sample. The load apparatus is always modeled by an analogous "elastic spring" as illustrated in Figure 1. Consequently, the load apparatus accumulates substantial elastic energy that, during strain softening after the peak stress, may trigger catastrophic rupture of a rock sample.

As shown in Figure 6, there are two typical rupture modes: catastrophic and gradual rupture observed in experiments. At the catastrophic point, the slope of the tangent line of the $F-u$ curve is $-k$ (the stiffness of load apparatus, see Figure 6a) [*Cook*, 1965] and a sudden jump appears. If k is larger than the negative value of the minimum slope of the tangent line, there is no catastrophic rupture during the loading process, i.e. failure is gradual and the $F-u$ curve is continuous without jump (Figure 6b). Therefore, a stiffer or an infinitely rigid test apparatus is needed to obtain the complete stress-strain curve of a rock-like material [*Salamon*, 1970; *Hudson et al.*, 1972; *Jaeger and Cook*, 1979; *Hao et al.*, 2013]. In this paper, however, we take advantage of elasticity of the testing machine to represent the surrounding and compliant elastic environments, and observe precursors of the response quantity (deformation) in the vicinity of a catastrophic point.

Here, the condition of catastrophic rupture in experiments is controlled by two main factors: the stiffness ratio between the load apparatus and damage evolution of a specific sample. As is known, the lower the stiffness ratio between the testing machine and sample, the more catastrophic rupture happens [*Cook*, 1965; *Salamon*, 1970; *Hao et al.*, 2007; *Hao et al.*, 2013]. Black granite has the largest initial stiffness of 681 kN/mm, which is almost 3 times of the testing machine. The initial stiffness (283 kN/mm) of white marble is the lowest one that is close to the testing machine. Catastrophic rupture occurs on all granites because of their high stiffness. In contrast, only ~10% (14/146) experiments on white marbles lead to catastrophic rupture. In the case of yellow marbles, whose stiffness is between white marbles and granites, 3 in the 26 samples show gradual but not catastrophic rupture. The detailed experimental results are provided in Supporting Information.

3. Power-law singularity with changeable exponent

The rapid increase of the response function $R = du/dU$ ahead of the catastrophic point (see Figure 6c) illustrates an acceleration process of deformation. However, R is not divergent in gradual failure because of continuous variation of the curve of u versus U.

To clearly observe the accelerating response of deformation u in the vicinity of a catastrophic rupture point, Figure 7 plots the curve of the normalized response function R/R_{max} versus the normalized residual life $(1-U/U_F)$ in a double logarithmic graph for two typical samples, where catastrophic rupture occurred. The final linear portion in the double

logarithmic curve (see Figure 7) indicates that the acceleration behavior can be well described by the power-law relationship (equation (3)). In these two cases, the critical power-law exponent β_F is equal to -0.63 ± 0.02 for black granite and $\beta_F = -0.60 \pm 0.01$ for white marble, respectively. The linear least-squares fitting method is used to fit the value of β_F. During fitting, the data set is selected according to the best linear correlation and with as many data points as possible. Moreover, as shown in Figure 8, the power-law exponent β_F ranges between -1 and $-1/2$.

As a matter of fact, the curve of R/R_{max} versus $(1-U/U_F)$ in a double logarithmic graph is a convex curve nearby the rupture point as shown in Figure 7. In order to examine this characteristic, the slope of $\log_{10}(R/R_{max})$ versus $\log_{10}(1-U/U_F)$ is calculated in terms of a moving fitting window with a fixed number of data points as determined in fitting β_F (see Figure 9a) for individual sample. A series values of the slope can be obtained as the window approaching to the rupture point. It is seen from Figure 9b that the fitted slope goes across $-1/2$ and decreases monotonically to its lower limit β_F when approaching to catastrophic rupture. Clearly, this monotonically decreasing trend of the slope shows the convexity of the double logarithmic curve and provides us a hint to look for an approach to forecast catastrophic rupture.

4. Prediction of catastrophic rupture

4.1 Variation of reduced exponent

It should be mentioned that the exponent β_F in equation (3) is unknown before catastrophic rupture. The fitted process and results described in Section 3 are a retrospective analysis based on the known value of the rupture point U_F. In practice, however, to predict U_F beforehand by using an available data set of $R(U)$ is really what we need. For the sake of prediction, we rewrite the response function $R(U)$ by substituting the unknown real U_F with the real-time sampling endpoint U_t in equation (3) as the available data set of $R(U)$ from a certain moment, that is

$$R(U) = B_t \left(1 - U/U_t\right)^{\beta_t}, \tag{4}$$

where B_t and reduced exponent β_t are parameters corresponding to the displacement U_t at time t. In the actual sampling process, only the data up to t is captured and beyond which they are unavailable. Based on equation (4), the reduced exponent β_t can be fitted by the data in the vicinity of individual U_t. Then, as U_t approaching to U_F, we can get a series values of β_t. It is worth noting that, however, β_t is different from the evolving slope in Figure 9, which is fitted with moving windows based on equation (3). Here, it is obvious that $\beta_t = \beta_F$ when $U_t = U_F$. It is found that the reduced exponent β_t decreases to β_F as U_t approaching to U_F (Figure 10). Moreover, it goes across −1/2 before rupture. This variation of the reduced exponent β_t with the real-time extended endpoint U_t, together with the lowest value of power-law exponent (i.e., $\beta_F = -1$), gives us a guide to estimate the upper bound of U_F based on the

real-time available data set before catastrophic rupture.

4.2 The upper bound of rupture point

To illustrate how to make a practical prediction of catastrophic rupture, let us rewrite equation (4) as

$$R^{1/\beta_t}(U) = C(U_t - U), \tag{5}$$

where $C = B_t^{1/\beta_t}/U_t$ is a constant. It indicates that the function $R^{1/\beta_t}(U)$ should present a linear relationship with U and $R^{1/\beta_t} = 0$ when $U = U_t$.

Since β_t decreases monotonically to β_F and the lowest value of β_F is −1, the upper bound of U_F (denoted as U_F) can be obtained, based on the same data set ended at U_t by substituting β_t with −1 in $R^{1/\beta_t}(U)$. As what we did for the case with β_t, the function $R^{-1}(U)$ is calculated based on the same data set used in fitting β_t and then the linear fitted result of $R^{-1}(U)$ can be obtained. Furthermore, U_F is determined by extrapolating the linear fitting of $R^{-1}(U)$ to zero. Therefore, the real rupture point U_F is constrained in the range of $[U_t, U_F]$.

To demonstrate the process and results, three successive stages with three data sets ended at different U_t for a white marble sample are illustrated in Figure 11. It is shown that R^{1/β_t} does vary linearly with U but R^{-1} varies a bit concavely, where β_t is the fitted exponent by equation (4) and the data up to U_t. So, these two curves of R^{1/β_t} and R^{-1} are the envelopes of the curve R^{1/β_F}. The curve of R^{1/β_t} has the same intersection point U_t at the abscissa, which provides a lower bound of U_F. Moreover, the intersection extrapolated from the linear fitting of $R^{-1}(U)$ with the abscissa gives an upper bound U_F. It is seen that U_F consistently

converges to U_F (see Figure 11 and red circles in Figure 12) and the range of $\left[U_t, U_F\right]$ becomes narrower as U_t approaching to the real rupture point.

The number of data points used for the above predictions are fixed as the same as that used in fitting β_F. As shown in Figure 11, this leads to that R^{-1} varies concavely. Thus, an alternative method that the linear fitting can be performed according to the best linear correlation of the final approximate linear part of R^{-1} versus U up to individual U_t. The predicted value $\widetilde{U}_F'$ of U_F is determined as the intersection with the abscissa axis, by linearly extrapolating the fitted straight line to zero. It is seen from Figure 12 that this method gives a more accurate prediction. Based on these estimations of $\widetilde{U}_F'$, the value of β_F can be accordingly estimated (see Figure 12d) by using equation (3).

5. Discussion

5.1 Energy criterion for catastrophic rupture and its kinematic counterpart

The above reported tests can be illustrated as an elastic system consisting of a sample and an elastic testing machine with the spring constant k in series (see Figure 13). Thus, the displacement U of the crosshead of the testing machine is the combination of the deformation u of the deformed sample and u_e of the load apparatus, that is

$$U = u + u_e = u + F(u)/k, \tag{6}$$

where k is the stiffness of the load apparatus. Derivatives of both sides of equation (6) gives that

$$\begin{cases} \dfrac{dU}{du} = 1 + \dfrac{1}{k}\dfrac{dF(u)}{du} \\ \dfrac{d^n U}{du^n} = \dfrac{1}{k}\dfrac{dF^n(u)}{du^n}, (n \geq 2) \end{cases}. \tag{7}$$

This means that all $n \geq 2$ order derivatives of $U(u)$ and $F(u)$ with respect to u are the same except for a constant k. Therefore, all discussion on force $F(u)$ can be replaced with $U(u)$, which is more easily measured in geo-field as well as in laboratory.

At the catastrophic point, the energy release made by the elastic load apparatus is able to compensate the required dissipative energy needed in the deformed sample without the input of external work [*Cook*, 1965; *Salamon*, 1970; *Hao et al.*, 2007; *Hao et al.*, 2010], that is

$$dW = 0, \tag{8}$$

where dW is an increment of external work. This energy criterion for catastrophic rupture can be rewritten as

$$dW = F \cdot dU = F \cdot (du + du_e) = F \cdot (du + dF/k) = 0. \tag{9}$$

Then, the catastrophic rupture point can be decided by

$$\left.\frac{dF(u)}{du}\right|_{\mathrm{F}} = -k. \tag{10}$$

[*Cook*, 1965; *Salamon*, 1970; *Hao et al.*, 2007; *Hao et al.*, 2010]. Geometrically, this form of energy criterion can be interpreted by the tangency of the force-displacement curve $F(u)$ through an elastic straight line with the slope of negative stiffness $-k$ at the rupture point (see Figure 13). In fact, if a rupture process follows a straight line with the slope $-k$, it always yields the energy criterion $dW = 0$, namely, self-sustained rupture.

Substituting equation (7) into equation (10), we can get the kinematic counterpart of the energy criterion for catastrophic rupture, that is

$$\left.\frac{dU}{du}\right|_{\mathrm{F}} = 0 \text{, or } \left. R\right|_{\mathrm{F}} = \left.\frac{du}{dU}\right|_{\mathrm{F}} = \infty . \tag{11}$$

Therefore, the tangency of the force-displacement curve $F(u)$ with the elastic straight line (equation (10)) converts to the tangency of the curve $u(U)$ with the straight line of $U = U_{\mathrm{F}}$ (equation (11)) at the rupture point. Consequently, the energy criterion of catastrophic rupture governs the singularity of the response function R at a catastrophic point.

In laboratory tests, it is convenient to monitor both the temporal evolution of stored energy in the load apparatus by measuring $(U-u)$, and the response R (the force-displacement curve that illustrates the state of rock samples). However, it is worth noting that, in nature and practical engineering, fault rupture or instability is much more complex than such a simplified system. It should be also mentioned that the behavior discussed here is of catastrophic rupture and very different from the well-defined 'critical' one of phase transformation in statistical physics.

5.2 The range of power-law exponent and its physical implication

Since $dU/du = 0$ at the rupture point U_{F} (equation (11)), the relationship between $(1-U/U_{\mathrm{F}})$ and $(1-u/u_{\mathrm{F}})$ can be approximated by a power function with $\lambda > 1$ in the vicinity of the catastrophic point, that is

$$\left(1-U/U_{\mathrm{F}}\right) = B_0 \left(1-u/u_{\mathrm{F}}\right)^{\lambda} \tag{12}$$

or

$$y = B_0 x^{\lambda}, \tag{13}$$

where B_0 and λ are two parameters, $x = (1-u/u_F)$, and $y = (1-U/U_F)$, respectively (see Figure 14a). Here, u_F represents the response quantity u at the catastrophic point. Then, $R = du/dU = B_F\left(1-U/U_F\right)^{\beta_F}$ (equation (3)) can be deduced with $B_F = u_F \Big/ \left(\lambda U_F \sqrt[\lambda]{B_0}\right)$ and $\beta_F = \frac{1}{\lambda} - 1 = -\frac{1}{2}$.

As shown in Figure 13 and Figure 14a, the curves of $F(u)$ and $u(U)$ exhibit a finite curvature at the rupture point ($x = y = 0$). Thus, we have $\lambda \geq 2$ (see Figure 14b). The result of $\lambda = 2$ (namely, $\beta_F = \frac{1}{\lambda} - 1 = -\frac{1}{2}$) can be derived in terms of series expansion [*Jin et al.*, 2012]. In series expansion, the first term of the series equals to zero due to energy criterion and the other order terms higher than the second one are omitted. Thus, the range of λ being $[2, +\infty)$ leads β_F to fall into $(-1, -1/2]$ (see Figure 14c). This is consistent with the experimental results in Figure 8.

According to equation (7), the tangency of $U(u)$ to the straight line $U = U_F$ has the same n-th order contact [*Porteous*, 2001] as the tangent of $F(u)$ and the corresponding straight line with the slope $-k$. Thus, the variation of λ (or β_F) is a reflection of the higher-order behavior of the loading curve nearby the rupture point. However, the energy criterion for catastrophic rupture is only a constraint on the first order derivative of the loading curve (equations (7) and (10)). Moreover, the variation of $\lambda \to \infty$ (or $\beta_F \to -1$) indicates the closeness between the loading curve $F(u)$ and the straight line with the slope $-k$ near the rupture point (see Figure

13 and Figure 14b). The greater λ (i.e., the closer to its lowest value −1 of the power-law exponent β_F), the closer to the rupture process without work input the loading process becomes. That is, the changeable power-law exponent β_F represents different-order contact to a catastrophic rupture process without external work input.

6. Conclusions

In the present experiments of granites and marbles under quasi-static uniaxial and unconfined compression, the power-law exponent of the response function at catastrophic rupture ranges from −1/2 to −1. This is verified by an analytical discussion based on a smoothly continuous model. Essentially, the power-law singularity is governed by the energy criterion and can be interpreted with a power function approximation. It is also demonstrated that, as the exponent is close to its lowest value −1, rocks are prone to catastrophic rupture without work input.

Practically, the reduced power-law exponent fitted with the real-time extended endpoint of sampling data set goes across −1/2 and decreases monotonically to its lower limit β_F in the vicinity of the catastrophic rupture point. Based on this relationship and the lowest value of the power-law exponent (−1), there is a constraint to the upper bound of the catastrophic rupture point U_F. This predicted upper bound together with the real-time sampling data set constitutes a predictive interval. With the extension of the sampling data set, the predicted interval becomes narrower and the predicted upper bound moves toward U_F. This approach

provides an unceasingly improving prediction of catastrophic rupture in real-time.

Acknowledgements

This work was supported by the National Natural Science Foundation of China (Grant Nos. 11372316, 11772332, 11432014 and 11672258), the National Basic Research Program of China (Grant no. 2013CB834100), the Strategic Priority Research Program of the Chinese Academy of Sciences (XDB22040501), the Opening Fund of State Key Laboratory of Nonlinear Mechanics (LNM) , and the Open Fund of State Key Laboratory for GeoMechanics and Deep Underground Engineering, China University of Mining & Technology (Beijing) (SKLGDUEK1516). Computations were performed on the LNMGrid of the LNM and the ScGrid of Supercomputing Center, Computer Network Information Center of the Chinese Academy of Sciences. Users can access the data from the Supporting Information.

References

Abaimov, S. G., and J. P. Cusumano (2014), Nucleation phenomena in an annealed damage model: Statistics of times to failure, *Phys. Rev. E*, *90*(6), 062401, doi:10.1103/PhysRevE.90.062401.

Bak, P., and C. Tang (1989), Earthquakes as a self-organized critical phenomenon, *J. Geophys. Res.*, *94*(B11), 15635–15637, doi:10.1029/JB094iB11p15635.

Bell, A. F., J. Greenhough, M. J. Heap, and I. G. Main (2011), Challenges for forecasting based on accelerating rates of earthquakes at volcanoes and laboratory analogues, *Geophys. J. Int.*, *185*(2), 718–723, doi:10.1111/j.1365–246X.2011.04982.x.

Bell, A. F., M. Naylor, and I. G. Main (2013), The limits of predictability of volcanic eruptions from accelerating rates of earthquakes, *Geophys. J. Int.*, *194*(3), 1541–1553, doi:10.1093/gji/ggt191.

Ben-Zion, Y., and V. Lyakhovsky (2002), Accelerated Seismic Release and Related Aspects of Seismicity Patterns on Earthquake Faults, *Pure Appl. Geophys.*, *10*(159), 2385–2412, doi:10.1007/978-3-0348-8197-5_12.

Boué, A., P. Lesage, G. Cortés, B. Valette, and G. Reyes-Dávila (2015), Real-time eruption forecasting using the material Failure Forecast Method with a Bayesian approach, *J. Geophys. Res.*, *120*(B4), 2143–2161, doi:10.1002/2014JB011637.

Bowman, D. D., G. Ouillon, C. G. Sammis, A. Sornette, and D. Sornette (1998), An observational test of the critical earthquake concept, *J. Geophys. Res.*, *103*(B10), 24359–24372, doi:10.1029/98JB00792.

Brace, W. F., and J. D. Byerlee (1966), Stick-slip as a mechanism for earthquakes, *Science*, *153*(3739), 990–992, doi:10.1126/science.153.3739.990.

Bufe, C. G., S. P. Nishenko, and D. J. Varnes (1994), Seismicity trends and potential for large earthquakes in the Alaska-Aleutian region, *Pure Appl. Geophys.*, *142*(1), 83–99, doi:10.1007/BF00875969.

Bufe, C. G., and D. J. Varnes (1993), Predictive modeling of the seismic cycle of the greater San Francisco Bay region, *J. Geophys. Res.*, *98*(B6), 9871–9883, doi:10.1029/93JB00357.

Carpenter, B. M., C. Marone, and D. M. Saffer (2011), Weakness of the San Andreas Fault revealed by samples from the active fault zone, *Nat. Geosci.*, *4*(4), 251, doi:10.1038/ngeo1089.

Cook, N. G. W. (1965), The failure of rock, *Int. J. Rock Mech. Min. Sci.*, *2*(4), 389–403, doi:10.1016/0148–9062(65)90004–5.

Cornelius, R. R., and P. A. Scott (1993), A materials failure relation of accelerating creep as empirical description of damage accumulation, *Rock Mech. Rock Eng.*, *26*(3), 233–252, doi:10.1007/BF01040117.

Cornelius, R. R., and B. Voight (1994), Seismological aspects of the 1989–1990 eruption at Redoubt Volcano, Alaska: the Materials Failure Forecast Method (FFM) with RSAM and SSAM seismic data, *J. Volcanol. Geoth. Res.*, *62*(1–4), 469–498, doi:10.1016/0377–0273(94)90048–5.

Girard, L., D. Amitrano, and J. Weiss (2010), Failure as a critical phenomenon in a progressive damage model, *Journal of Statistical Mechanics: Theory and Experiment*, *2010*(01), P01013, doi:10.1088/1742–5468/2010/01/P01013.

Guarino, A., S. Ciliberto, A. Garcimartın, M. Zei, and R. Scorretti (2002), Failure time and critical behaviour of fracture precursors in heterogeneous materials, *The European Physical Journal B - Condensed Matter and Complex Systems*, *26*(2), 141–151, doi:10.1140/epjb/e20020075.

Guarino, A., A. Garcimartín, and S. Ciliberto (1998), An experimental test of the critical behaviour of fracture precursors, *Eur. Phys. J. B*, *6*(1), 13–24, doi:10.1007/s100510050521.

Hao, S., C. Liu, C. Lu, and D. Elsworth (2016), A relation to predict the failure of materials and potential application to volcanic eruptions and landslides, *Sci. Rep.*, *6*, 27877, doi:10.1038/srep27877.

Hao, S., F. Rong, M. Lu, H. Wang, M. Xia, F. Ke, and Y. Bai (2013), Power-law singularity as a possible catastrophe warning observed in rock experiments, *Int. J. Rock Mech. Min. Sci.*, *60*, 253–262, doi:10.1016/j.ijrmms.2012.12.004.

Hao, S., H. Wang, M. Xia, F. Ke, and Y. Bai (2007), Relationship between strain localization and catastrophic rupture, *Theor. Appl. Fract. Mec.*, *48*(1), 41–49, doi:10.1016/j.tafmec.2007.04.006.

Hao, S., M. Xia, F. Ke, and Y. Bai (2010), Evolution of localized damage zone in heterogeneous media, *Int. J. Damage Mech.*, *19*(7), 787–804.

Hao, S., B. Zhang, and J. Tian (2012), Relaxation creep rupture of heterogeneous material under constant strain, *Phys. Rev. E*, *85*(1), 012501, doi:10.1103/PhysRevE.85.012501.

Hao, S., B. Zhang, J. Tian, and D. Elsworth (2014), Predicting time-to-failure in rock extrapolated from secondary creep, *J. Geophys. Res.*, *119*(3), 1942–1953, doi:10.1002/2013JB010778.

Heap, M. J., P. Baud, P. G. Meredith, A. F. Bell, and I. G. Main (2009), Time-dependent brittle creep in Darley Dale sandstone, *J. Geophys. Res.*, *114*(B7), 4288–4309, doi:10.1029/2008JB006212.

Helmstetter, A., D. Sornette, J.-R. Grasso, J. V. Andersen, S. Gluzman, and V. Pisarenko (2004), Slider-block friction model for landslides: Application to Vaiont and La Clapière landslides, *J. Geophys. Res.*, *109*(B2), doi:10.1029/2002JB002160.

Hudson, J. A., S. L. Crouch, and C. Fairhurst (1972), Soft, stiff and servo-controlled testing machines: a review with reference to rock failure, *Engineering Geology*, *6*(3), 155–189, doi:10.1016/0013–7952(72)90001–4.

Jaeger, J. C., and N. G. W. Cook (1979), *Fundamentals of rock mechanics*, 593 pp., Methuen & Co, LTD, London.

Jin, Y., M. Xia, and H. Wang (2012), Uncertainty and universality in the power-law singularity as a precursor of catastrophic rupture, *Sci. China Phys. Mech. Astron.*, *55*(6), 1098–1102, doi:10.1007/s11433–012–4727–4.

Kilburn, C. R. J. (2003), Multiscale fracturing as a key to forecasting volcanic eruptions, *J.*

Volcanol. Geoth. Res., *125*(3–4), 271–289, doi:10.1016/S0377–0273(03)00117–3.

Kilburn, C. R. J. (2012), Precursory deformation and fracture before brittle rock failure and potential application to volcanic unrest, *J. Geophys. Res.*, *117*(B2), doi:10.1029/2011JB008703.

Kilburn, C. R. J., and B. Voight (1998), Slow rock fracture as eruption precursor at Soufriere Hills Volcano, Montserrat, *Geophys. Res. Lett.*, *25*(19), 3665–3668, doi:10.1029/98GL01609.

Lavallée, Y., P. G. Meredith, D. B. Dingwell, K. U. Hess, J. Wassermann, B. Cordonnier, A. Gerik, and J. H. Kruhl (2008), Seismogenic lavas and explosive eruption forecasting, *Nature*, *453*(7194), 507, doi:10.1038/nature06980.

Li, V. C., and J. R. Rice (1983), Precursory surface deformation in great plate boundary earthquake sequences, *B. Seismol. Soc. Am.*, *73*(5), 1415–1434.

Lyakhovsky, V., and Y. Ben-Zion (2014), Damage–breakage rheology model and solid-granular transition near brittle instability, *J. Mech. Phys. Solids*, *64*, 184–197, doi:10.1016/j.jmps.2013.11.007.

Lyakhovsky, V., Y. Hamiel, and Y. Ben-Zion (2011), A non-local visco-elastic damage model and dynamic fracturing, *J. Mech. Phys. Solids*, *59*(9), 1752–1776, doi:10.1016/j.jmps.2011.05.016.

Main, I. G. (1999), Applicability of time-to-failure analysis to accelerated strain before earthquakes and volcanic eruptions, *Geophys. J. Int.*, *139*(3), F1–F6, doi:10.1046/j.1365–246x.1999.00004.x.

Nechad, H., A. Helmstetter, R. El Guerjouma, and D. Sornette (2005a), Andrade and critical time-to-failure laws in fiber-matrix composites: Experiments and model, *J. Mech. Phys. Solids*, *53*(5), 1099–1127, doi:10.1016/j.jmps.2004.12.001.

Nechad, H., A. Helmstetter, R. El Guerjouma, and D. Sornette (2005b), Creep ruptures in heterogeneous materials, *Phys. Rev. Lett.*, *94*(4), 045501, doi:10.1103/PhysRevLett.94.045501.

Porteous, I. R. (2001), *Geometric differentiation: for the intelligence of curves and surfaces*, 2 ed., 350 pp., Cambridge University Press, The Edinburgh Building, Cambridge CB2 2RU, UK.

Rundle, J. B., W. Klein, D. L. Turcotte, and B. D. Malamud (2000), Precursory seismic activation and critical-point phenomena, *Pure Appl. Geophys.*, *157*(11–12), 2165–2182, doi:10.1007/PL00001079.

Rundle, J. B., D. L. Turcotte, R. Shcherbakov, W. Klein, and C. Sammis (2003), Statistical physics approach to understanding the multiscale dynamics of earthquake fault systems, *Rev. Geophys.*, *41*(4), doi:10.1029/2003RG000135.

Salamon, M. D. G. (1970), Stability, instability and design of pillar workings, *Int. J. Rock Mech. Min. Sci.*, *7*(6), 613–631, doi:10.1016/0148–9062(70)90022–7.

Scholz, C. H. (1998), Earthquakes and friction laws, *Nature*, *391*(6662), 37, doi:10.1038/34097.

Smith, R., and C. R. J. Kilburn (2010), Forecasting eruptions after long repose intervals from

accelerating rates of rock fracture: The June 1991 eruption of Mount Pinatubo, Philippines, *J. Volcanol. Geoth. Res.*, *191*(1–2), 129–136, doi:10.1016/j.jvolgeores.2010.01.006.

Smith, R., P. R. Sammonds, and C. R. J. Kilburn (2009), Fracturing of volcanic systems: Experimental insights into pre-eruptive conditions, *Earth Planet. Sc. Lett.*, *280*(1), 211–219, doi:10.1016/j.epsl.2009.01.032.

Sornette, D., and C. G. Sammis (1995), Complex critical exponents from renormalization group theory of earthquakes: Implications for earthquake predictions, *J. Phys. I*, *5*(5), 607–619, doi:10.1051/jp1:1995154.

Toussaint, R., and S. R. Pride (2002a), Fracture of disordered solids in compression as a critical phenomenon. I. Statistical mechanics formalism, *Phys. Rev. E*, *66*(3), 036135, doi:10.1103/PhysRevE.66.036135.

Toussaint, R., and S. R. Pride (2002b), Fracture of disordered solids in compression as a critical phenomenon. II. Model Hamiltonian for a population of interacting cracks, *Phys. Rev. E*, *66*(3), 036136, doi:10.1103/PhysRevE.66.036136.

Toussaint, R., and S. R. Pride (2002c), Fracture of disordered solids in compression as a critical phenomenon. III. Analysis of the localization transition, *Phys. Rev. E*, *66*(3), 036137, doi:10.1103/PhysRevE.66.036137.

Toussaint, R., and S. R. Pride (2005), Interacting damage models mapped onto Ising and percolation models, *Phys. Rev. E*, *71*(4), 046127, doi:10.1103/PhysRevE.71.046127.

Voight, B. (1988), A method for prediction of volcanic eruptions, *Nature*, *332*(6160), 125–130, doi:10.1038/332125a0.

Voight, B. (1989), A relation to describe rate-dependent material failure, *Science*, *243*(4888), 200–203, doi:10.1126/science.243.4888.200.

Voight, B., and R. R. Cornelius (1991), Prospects for eruption prediction in near real-time, *Nature*, *350*(6320), 695–698, doi:10.1038/350695a0.

Weiss, J., L. Girard, F. Gimbert, D. Amitrano, and D. Vandembroucq (2014), (Finite) statistical size effects on compressive strength, *Proceedings of the National Academy of Sciences*, *111*(17), 6231–6236, doi:10.1073/pnas.1403500111.

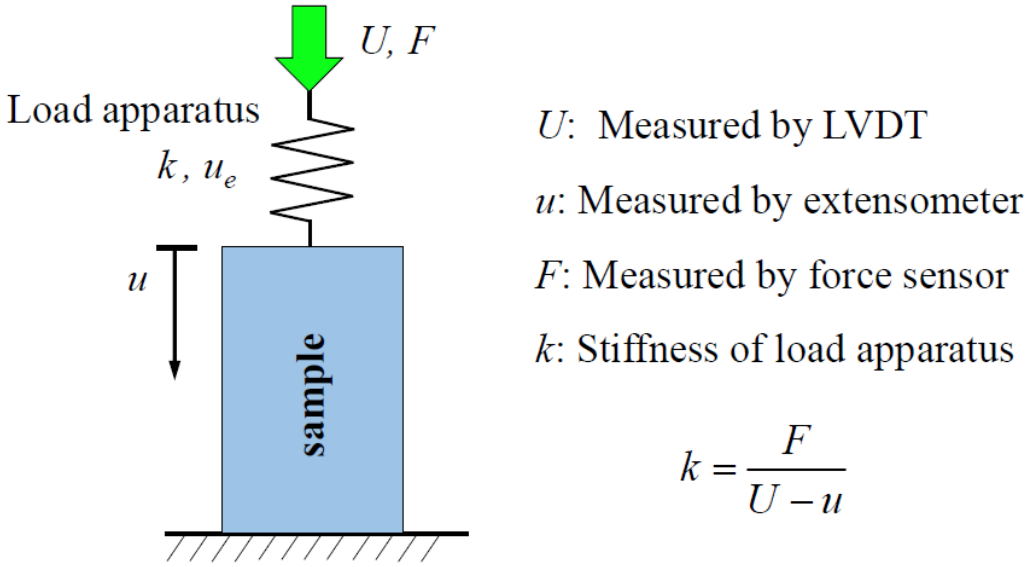

Figure 1. Schematic illustration of a system consisting of a load apparatus and a sample in series.

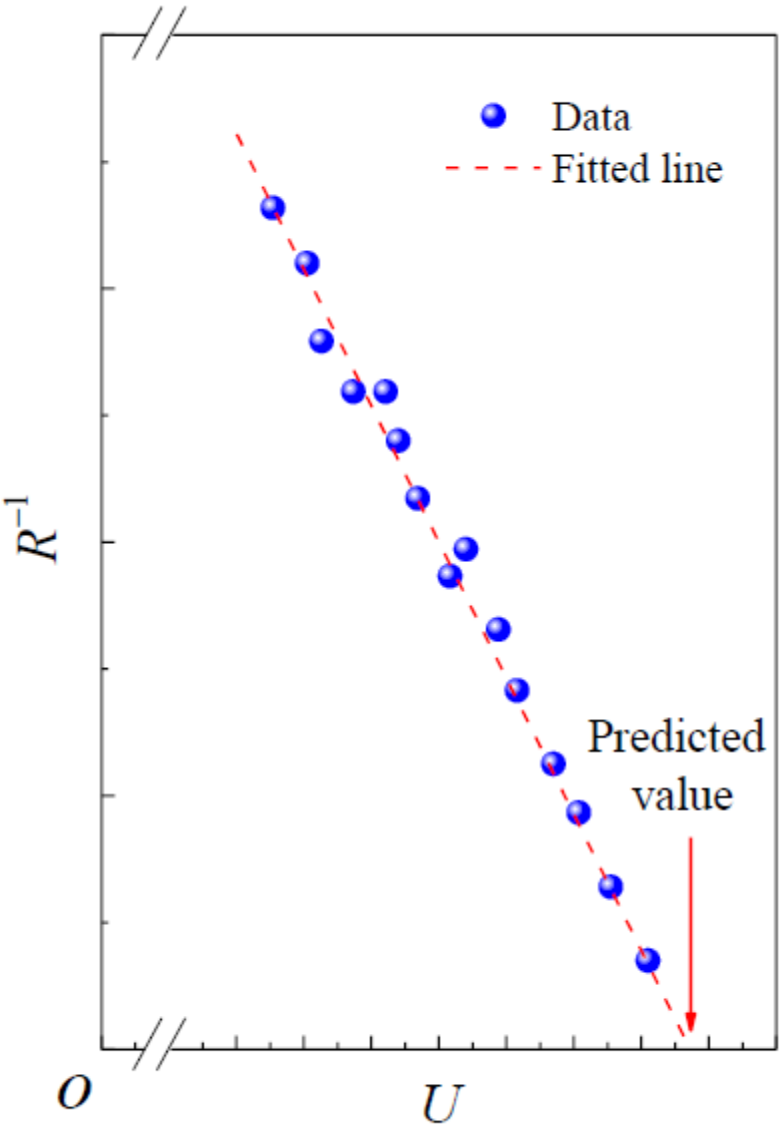

Figure 2. Illustration of a linear extrapolation to predict the failure time, which is the intersection point by extrapolating the best-fitting line of R^{-1} to the U-axis.

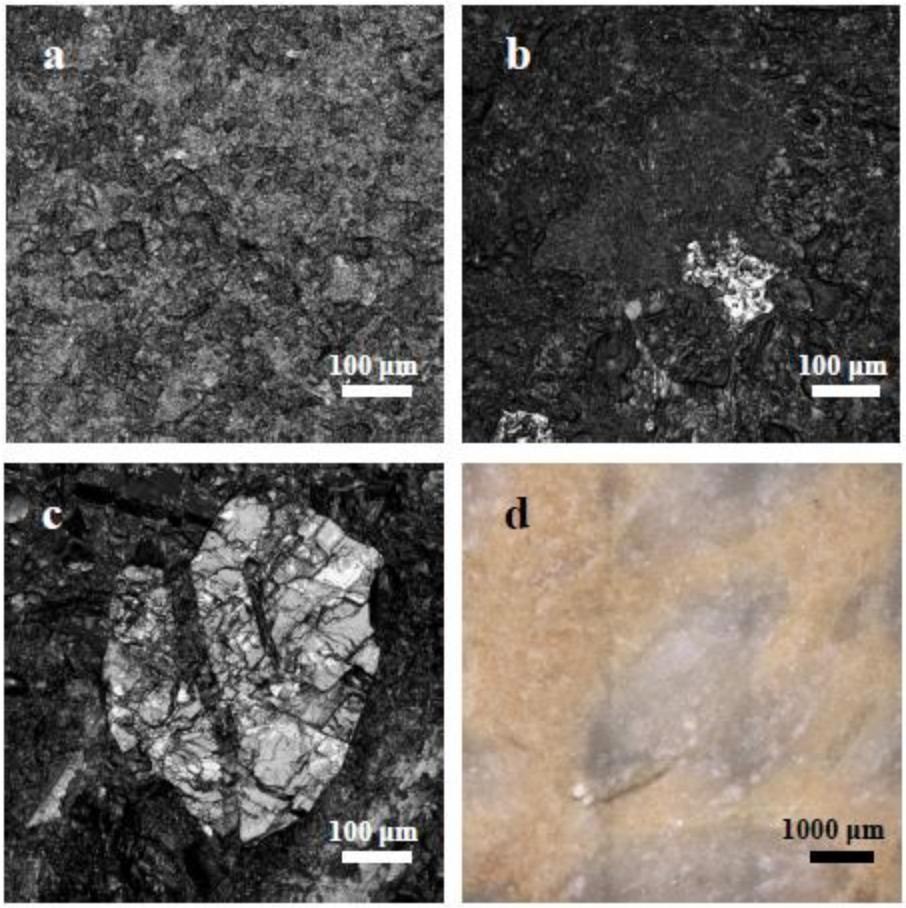

Figure 3. Optical microscope images of (a) an ordinary granite, (b) a black granite, (c) a white marble, and (d) a yellow marble before loading.

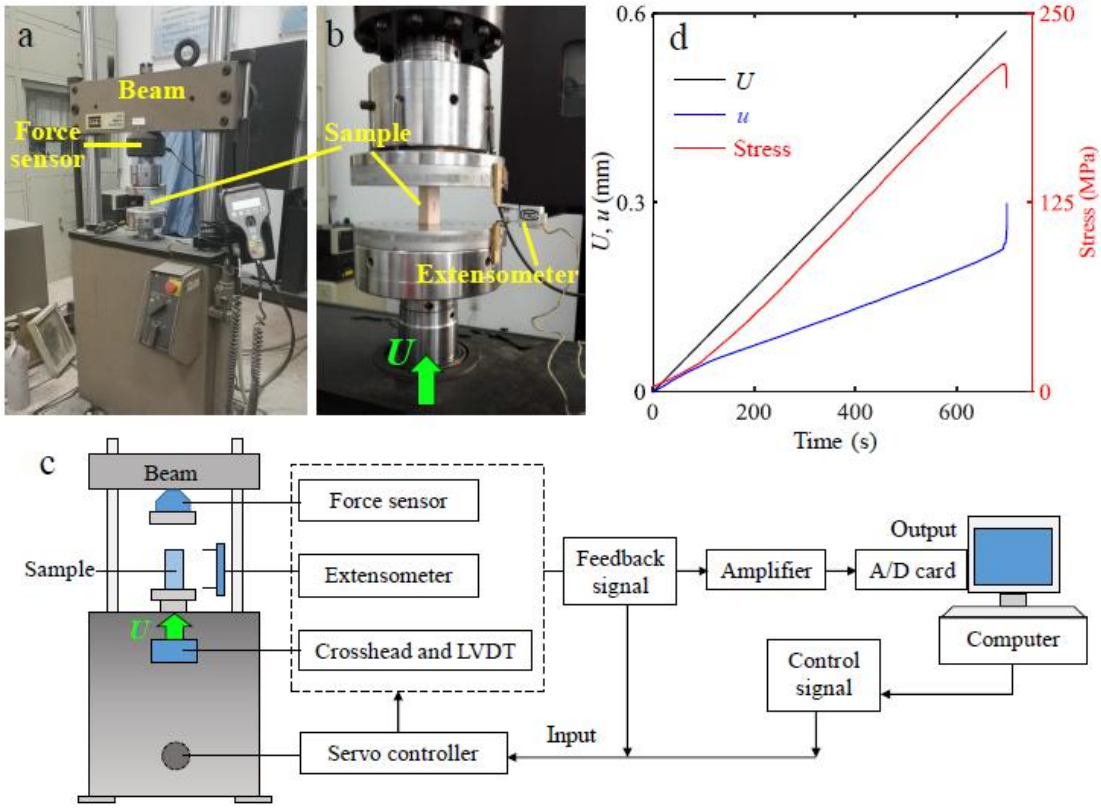

Figure 4. (a) The testing equipment (MTS810 testing system) for uniaxial compression tests and (b) its platens and extensometer, where *U* is the controlling displacement. (c) Schematic illustration of the testing and acquisition system. (d) The experimental protocol to illustrate the change of displacement, deformation and stress of a sample versus time.

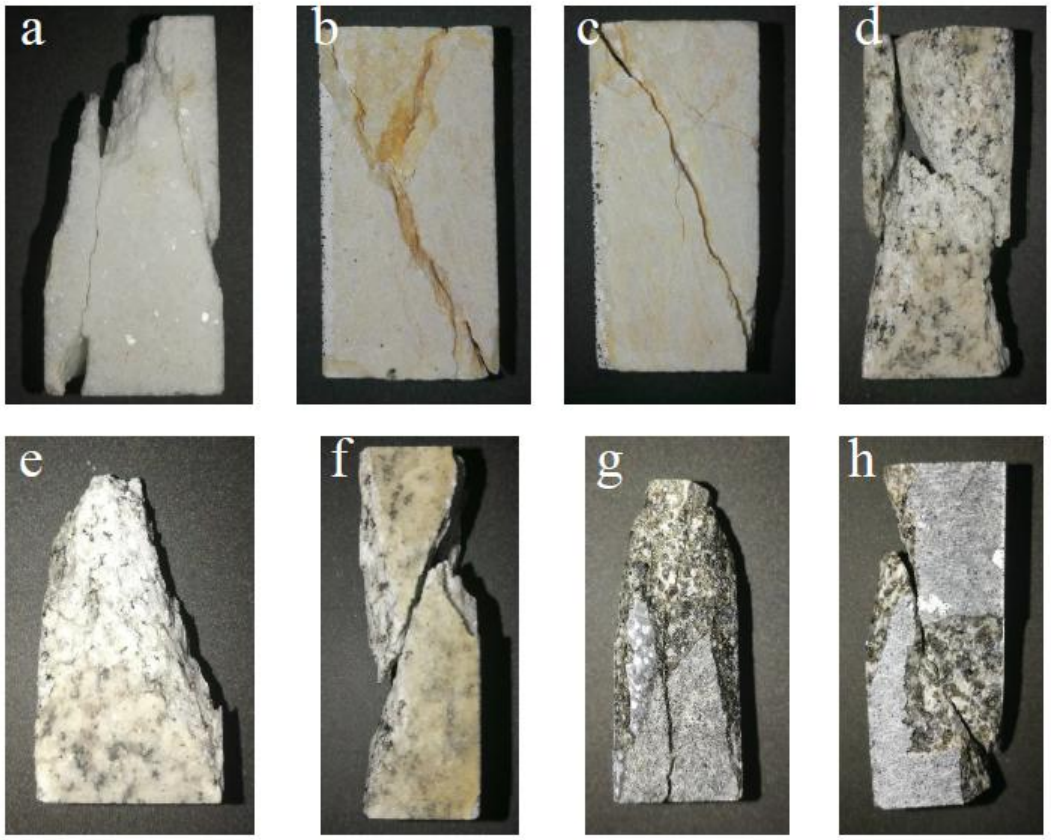

Figure 5. Typical rupture modes of tested samples of (a−c) marble and (d−h) granite.

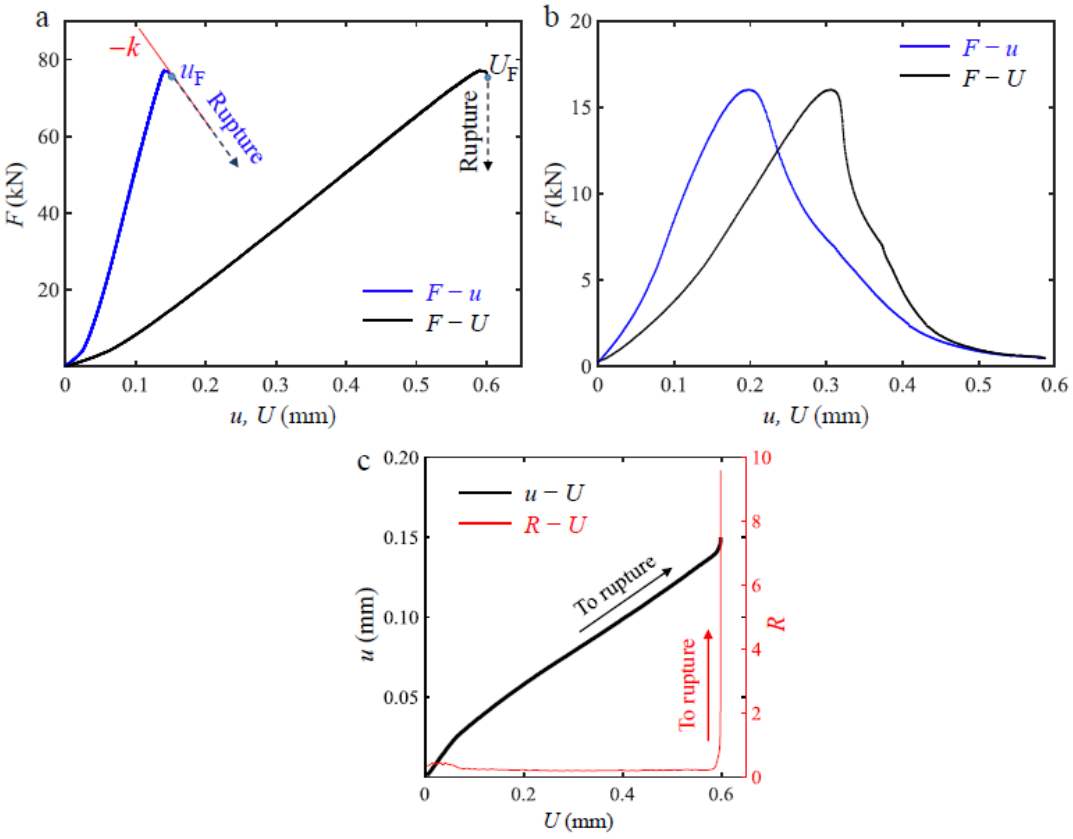

Figure 6. Differences of two typical rupture modes: catastrophic and gradual rupture. The different curves of $F-U$ and $F-u$ in samples with catastrophic rupture (a) but gradual failure (b). Additionally, (c) the singular trend of $u-U$ and $R-U$ before catastrophic rupture.

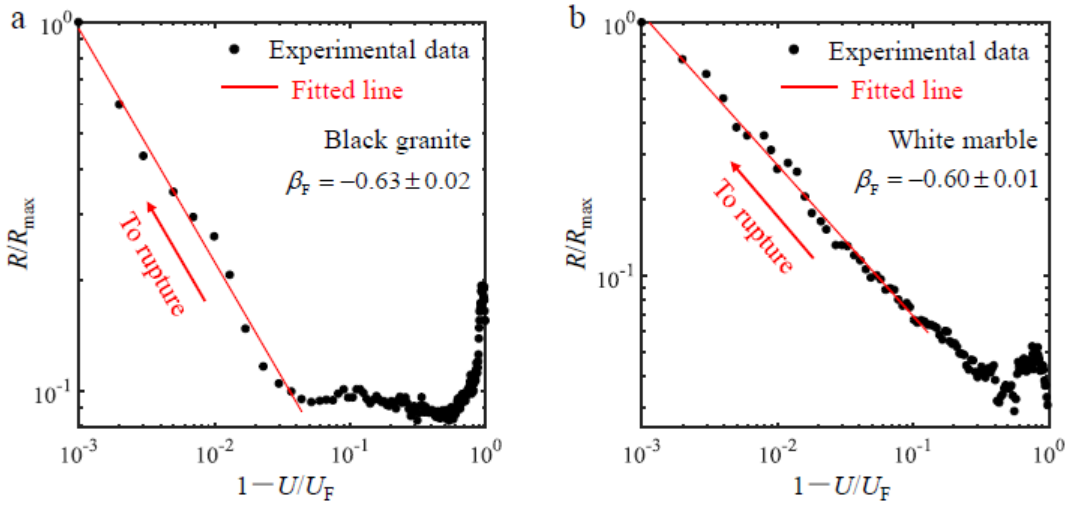

Figure 7. Power-law singularity of the normalized response function R/R_{max} for (a) a black granite and (b) a white marble, where R_{max} represents the maximum value of R at the rupture point.

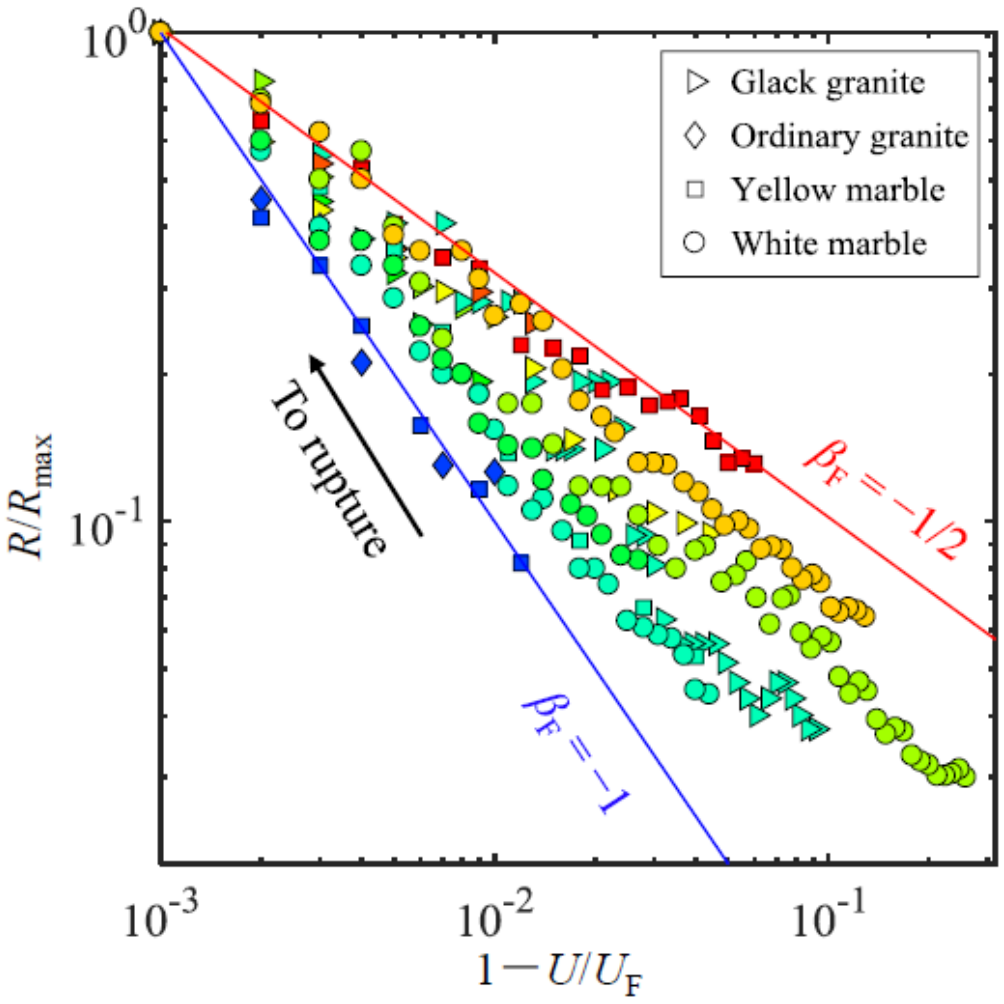

Figure 8. The range of the power-law exponent β_F. Each kind of symbols represents a specific kind of samples. Color represents different values of the slope in the vicinity of failure (i.e., β_F) that ranges between −1 and −1/2.

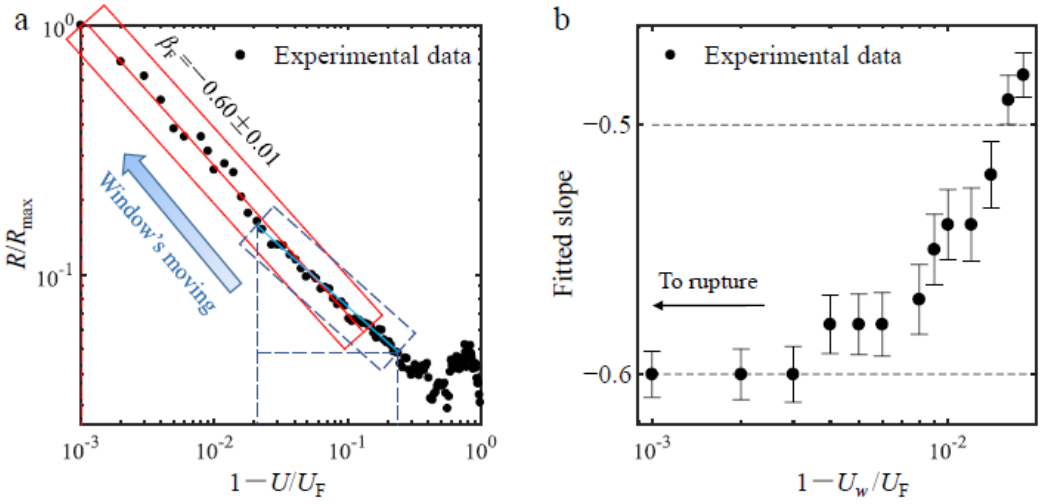

Figure 9. An example of a white marble in Figure 6b to show the fitting process and results of the slope by using a moving fitting window. (a) The fitting process with a moving window and (b) the fitted results and error bars of the slope of $\log_{10}(R/R_{max})$ versus $\log_{10}(1-U/U_F)$ by using a moving fitting window with a fixed number of data points inside.

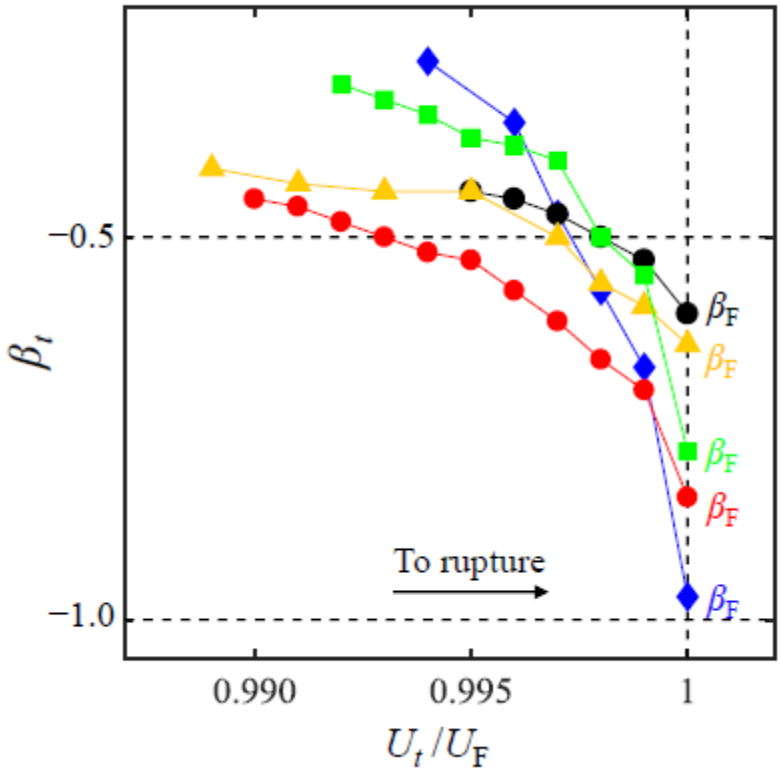

Figure 10. The reduced exponent β_t decreases to β_F as U_t approaching to U_F (five marble samples).

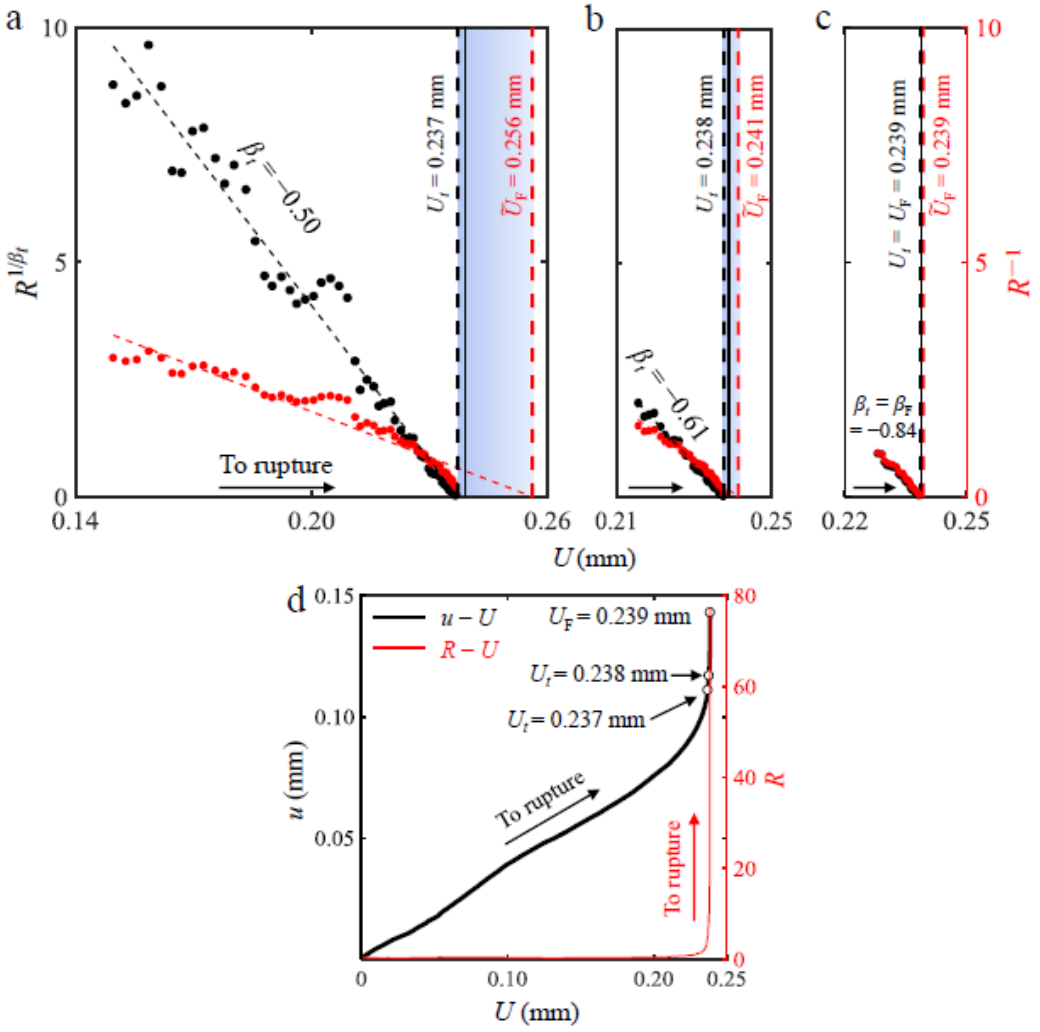

Figure 11. Predicted rupture point U_F and its update in real-time for a white marble. (a) U_t = 0.237 mm, β_t = −0.50, and $U_F = 0.256$ mm. (b) U_t = 0.238 mm, β_t = −0.61, and $U_F = 0.241$ mm. (c) U_t = U_F = 0.239 mm, β_t = β_F = −0.84, and U_F = 0.239 mm. In comparison, the experimentally observed U_F is shown by a vertical black solid line. The black solid circles denote $R^{1/\beta_t}(U)$ based on data set ended at U_t and the red ones are $R^{-1}(U)$. (d) The values of U_t used for prediction marked on the curves of u−U and R−U.

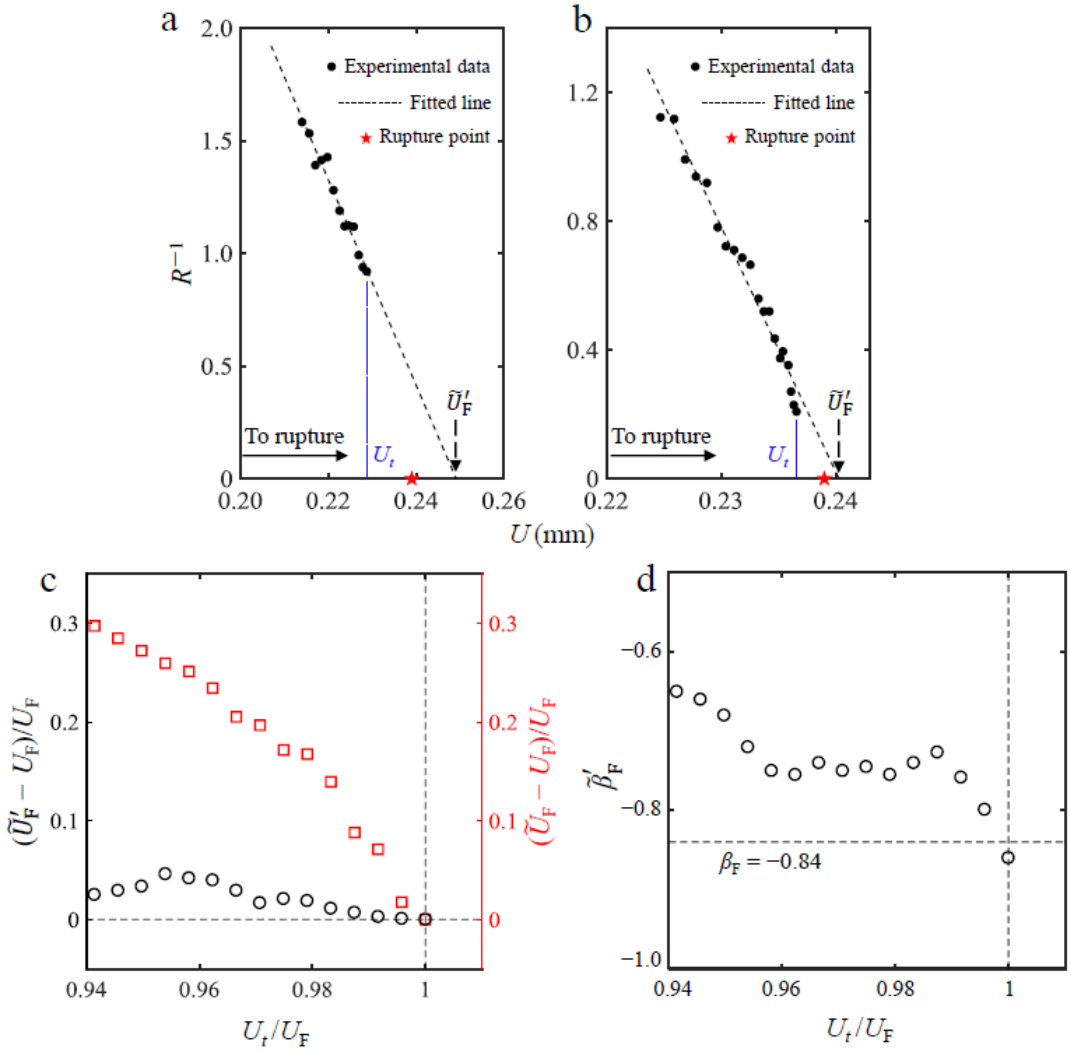

Figure 12. The predicted results by using the approximate linear part of R^{-1}. Two predicted results in the time sequence of (a) U_t = 0.229 mm and (b) U_t = 0.237 mm. (c) The comparison of two predicted results of U_F by using the method mentioned here (circle) and that in Figure 10 (square), respectively. (d) $\tilde{\beta}'_F$ estimated by using equation (3) and the predicted values of U_F shown by circles in Figure 11c.

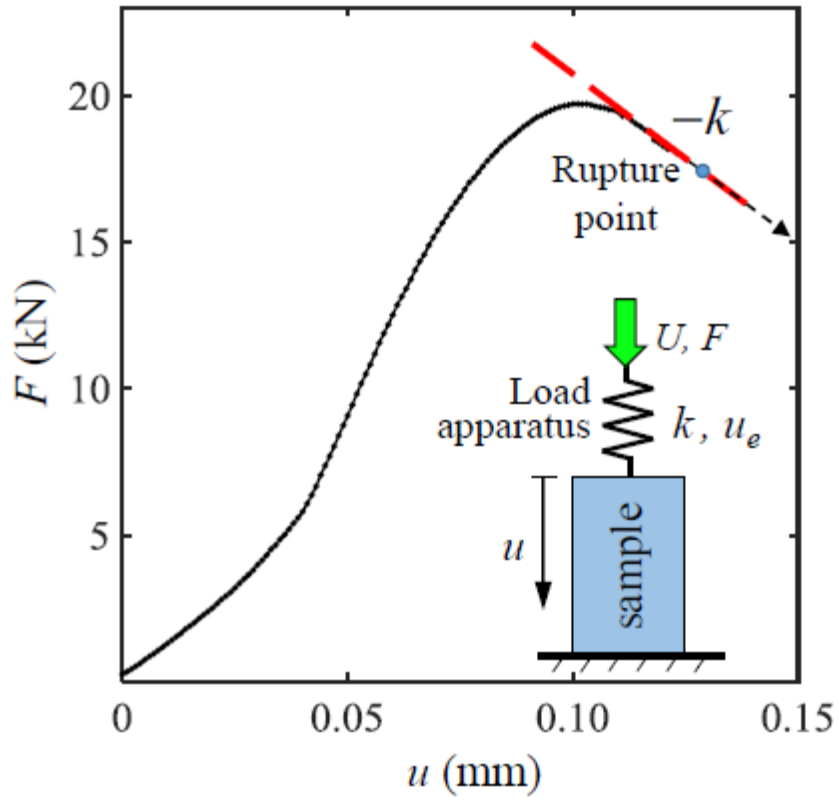

Figure 13. Schematic diagram showing the energy criterion (equation (10)) for catastrophic rupture, where inset is a simplified model of the sample and load apparatus in series.

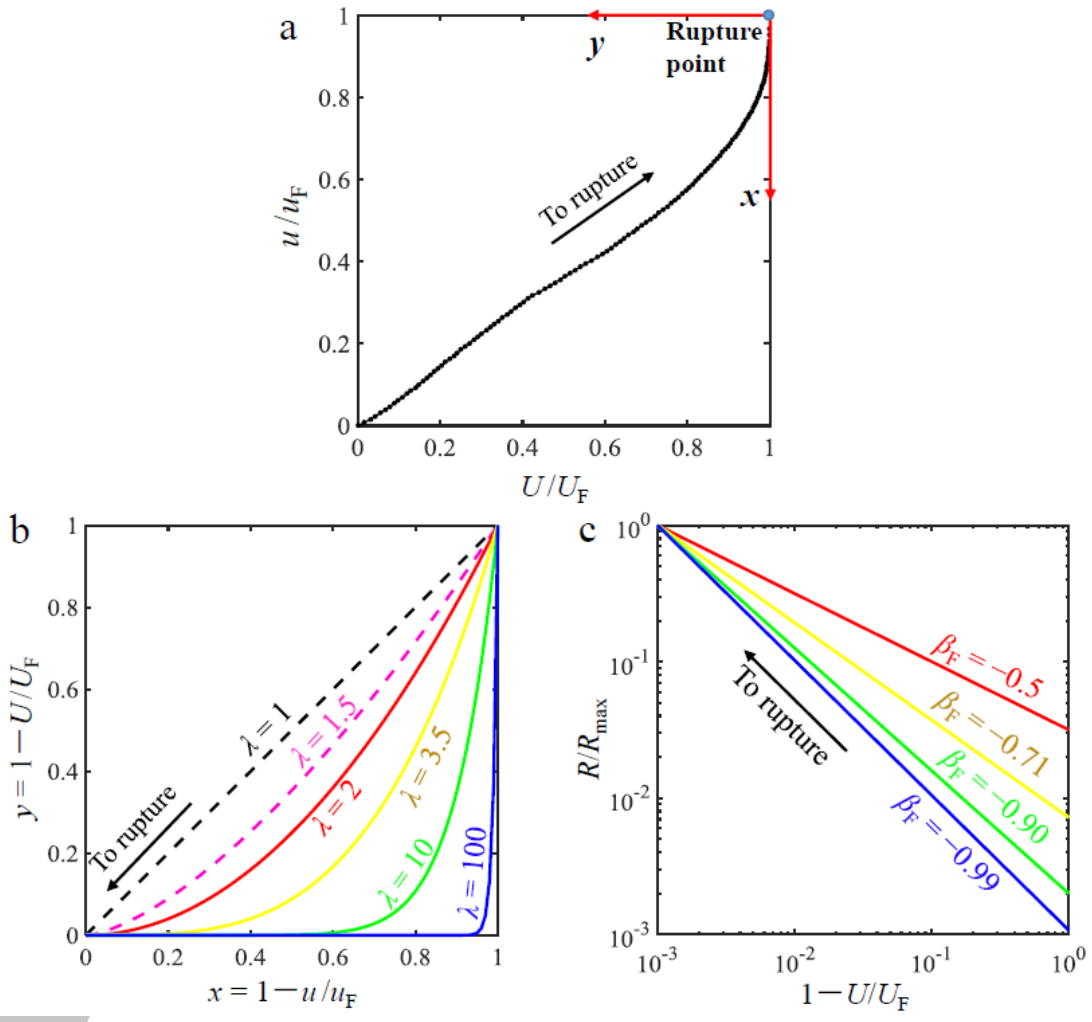

Figure 14. Illustration of a power function approximation in the vicinity of the catastrophic point ($x = y = 0$). (a) Evolution of the normalized deformation u/u_F versus the normalized displacement U/U_F of a sample. (b) Variation of $y = (1-U/U_F)$ versus $x = (1-u/u_F)$ with different values of exponent λ, and (c) the relationship between $\log_{10}(R/R_{max})$ and $\log_{10}(1-U/U_F)$ with $\beta_F\,(= 1/\lambda-1)$.

Table 1. Parameters of two kinds of samples, where the values in parentheses represent the number of samples subjecting to catastrophic rupture.

Sample	Total number	Sample size (mm^3)	Initial stiffness (kN/mm)	Density (kg/m^3)
Black granite	21 (21)	16×18×40	681	3081.6
Ordinary granite	59 (59)	20×15×40	398	2625.0
Yellow marble	26 (23)	16×18×40	361	2534.7
White marble	146 (14)	20×20×40	283	2867.2